NUMERICAL INVESTIGATION ON THE FLOW AND POLLUTANT DISPERSION OVER 3D TOPOGRAPHY

André Augusto Isnard
Pontifícia Universidade Católica do Rio de Janeiro - Departamento de Engenharia Mecânica
Av. Marquês de São Vicente 225 , CEP22453-900, Rio de Janeiro, RJ, Brazil.
isnard@mec.puc-rio.br

Marcos Sebastião de Paula Gomes
Pontifícia Universidade Católica do Rio de Janeiro - Departamento de Engenharia Mecânica
Av. Marquês de São Vicente 225 , CEP22453-900, Rio de Janeiro, RJ, Brazil.
mspgomes@mec.puc-rio.br

Abstract. The work investigated numerically the stably stratified flow and pollutant dispersion over a three dimensional topography. The numerical procedure, based in the finite volume formulation, included the Reynolds stress model for turbulence and a two-layer zonal approach for near-wall treatment. The commercial code Fluent (Version 6.0.12) was used for performing the simulations. The numerical results were compared with wind tunnel experiments. Comparisons were also made with results obtained with the traditional $k - \varepsilon$ model for turbulence.

Keyword: numerical modeling, atmospheric pollution

1. Introduction

The study of wind field over hills has been object of intensive study over the last two decades, from both a theoretical standpoint and via field and laboratory experiments. The understanding of the physical progress by which the topography changes both the mean wind and the turbulence structure has progressed considerably. The development of powerful computers has led to the possibility of computing such flows by the integration of the modeled and time-averaged Navier-Stokes equations.

Castro and Apsley (1997) developed a suitably modified $k - \varepsilon$ turbulence model and compared numerical results with laboratory data for flow and dispersion over two-dimensional hills of various slope and submerged in a neutrally stable boundary layer. It was shown that the employed model produced reasonable agreement for the mean flow behavior, but somewhat lower values for the turbulent kinetic energy and the lateral plume spread. Apsley and Castro (1997) used a finite volume code to calculate flow and dispersion in stably-stratified flow over topography. They applied a length scale limiting strategy suitable for atmospheric boundary layer applications. A detailed simulation was undertaken of one particular case-study hour in the Cinder Cone Butte dispersion experiment and concentrations compared with field and laboratory data.

Boçon and Maliska (1998) extended and applied a non-isotropic turbulence model to three dimensional stably stratified flows. The model was derived from the algebraic stress model, but retaining the simplicity of the "eddy viscosity" concept of first order models. Numerical solutions were compared with wind tunnel experiments and also against the results obtained with the standard $k - \varepsilon$ model. In Boçon and Maliska (1999), the "modified $k - \varepsilon$" (as named by the authors) model was evaluated against a full scale dispersion experiment. Three dimensional stably stratified flows and tracer dispersion over Cinder Cone Butte (USA) were computational simulated.

The turbulence anisotropy is a very relevant feature on environmental flows. The vertical fluctuations are much influenced by the temperature stratification, but the horizontal fluctuations are not. In unstable flows, the buoyancy forces tend to increase the vertical fluctuations, while in stably stratified flows the vertical fluctuations are inhibited. So, it is expected that isotropic turbulence models do not success in reproducing anisotropic turbulent diffusion.

An alternative approach for situations in which the anisotropy of turbulence has a dominant effect on the mean flow is the Reynolds stress model. This turbulence model involves the solution of transport equations for each component of the Reynolds stress tensor. The larger CPU time and memory required for the Reynolds stress model (*rsm*) has been an obstacle to its employment for engineering applications.

This study is part of a main body of research in the field of atmospheric pollutant dispersion. In a previous work (Isnard and Gomes, 2002), it was investigated the pollutant dispersion in the atmospheric microscale through the employment of two different approaches: the computational fluids dynamics (CFD) and by the Gaussian modeling following the North-American Environmental Protection Agency (U.S. E.P.A.) recommendations.

In the present work it was investigated numerically the stably stratified flows and pollutant dispersion over three

dimensional topography. The numerical procedure, based in the finite volume formulation, included the Reynolds Stress model for turbulence and a two-layer zonal approach for near-wall treatment. The commercial code Fluent (Version 6.0.12) was used for performing the simulations. The numerical results were compared with wind tunnel experiments for which the experimental data was available (Boçon and Maliska, 1998). Comparisons were also made with results obtained with the standard $k - \varepsilon$ model for turbulence. The influence of the turbulent near-wall treatments was investigated by the comparison between results obtained with the two-layer zonal approach and the logarithmic wall function.

2. Model Description

2.1. Flow Field

The governing equations for the flow are the conservation of mass Eq. (1) and momentum Eq.(2).

$$\frac{\partial}{\partial x_i}(\rho u_i) = 0 \tag{1}$$

$$\frac{\partial}{\partial t}(\rho u_i) + \frac{\partial}{\partial x_j}(\rho u_j u_i) = \frac{\partial}{\partial x_j}\left\{-\delta_{ij}p + \mu\left[\left(\frac{\partial u_i}{\partial x_j} + \frac{\partial u_j}{\partial x_i}\right) - \frac{2}{3}\delta_{ij}\frac{\partial u_l}{\partial x_l}\right] - \overline{(\rho u_j)'u'_i}\right\} + \rho g_i \tag{2}$$

2.2. Turbulence Modeling

Two turbulence models were tested and compared, the $k - \varepsilon$ and Reynolds stress model for turbulence. The standard $k - \varepsilon$ model is sufficiently well-known not to require too detailed a description here. It is based on the eddy viscosity concept, which relates the Reynolds stresses to the gradient of the velocity components as

$$-\overline{(\rho u_j)'u'_i} = \mu_t\left(\frac{\partial u_i}{\partial x_j} + \frac{\partial u_j}{\partial x_i}\right) - \frac{2}{3}\delta_{ij}\left(\mu_t\frac{\partial u_l}{\partial x_l} + \frac{\rho}{2}\overline{u'^2_l}\right) \tag{3}$$

where the turbulent viscosity μ_t is defined as

$$\mu_t = \rho C_\mu \frac{k^2}{\varepsilon} \tag{4}$$

2.2.2. The Reynolds Stress Model

The Reynolds stress model involves calculation of the individual Reynolds stress, $\overline{u'_i u'_j}$, using differential transport equations. The individual stresses are then used to obtain closure of the Reynolds-average momentum equation (Eq.1).

$$\underbrace{\frac{\partial}{\partial x_k}\left(\rho u_k \overline{u'_i u'_j}\right)}_{C_{ij} \equiv \text{Convection}} = \underbrace{-\frac{\partial}{\partial x_l}\left[\rho\overline{u'_i u'_j u'_k} + \overline{p(\delta_{kj}u'_i + \delta_{ik}u'_j)}\right]}_{D_{T,ij} \equiv \text{Turbulent Diffusion}} + \underbrace{\frac{\partial}{\partial x_k}\left[\mu\frac{\partial}{\partial x_l}(\overline{u'_i u'_j})\right]}_{D_{ij} \equiv \text{Molecular Diffusion}} +$$

$$\underbrace{-\rho\left(\overline{u'_i u'_k}\frac{\partial \overline{u}_j}{\partial x_k} + \overline{u'_i u'_k}\frac{\partial \overline{u}_i}{\partial x_k}\right)}_{P_{ij} \equiv \text{Stress Production}}\underbrace{-\rho\beta(g_i\overline{u'_j\theta} + g_j\overline{u'_i\theta})}_{G_{ij} \equiv \text{Buoyancy Production}} + \underbrace{\overline{p\left(\frac{\partial u'_i}{\partial x_j} + \frac{\partial u'_j}{\partial x_i}\right)}}_{\phi_{ij} \equiv \text{Pressure}}\underbrace{-2\mu\overline{\frac{\partial u'_i}{\partial x_k}\frac{\partial u'_j}{x_k}}}_{\varepsilon_{ij} \equiv \text{Dissipation}} \tag{5}$$

Of the various terms above, C_{ij}, $D_{L,ij}$, P_{ij} and F_{ij} do not require any modeling. However $D_{T,ij}$, G_{ij}, ϕ_{ij}, ε_{ij} need to be modeled to close the equations. The description of the modeling assumptions required to these terms can be found in (Fluent User's Guide, 2003).

In general, when the turbulent kinetic energy is needed for modeling a specific term, it is obtained by taking the trace of the Reynolds stress tensor

$$k = \frac{1}{2}\overline{u_i' u_i'}$$ (6)

In order to obtain boundary conditions for the Reynolds stress, a transport equation for the turbulence kinetic energy is solved. The dissipation rate scalar ε, required for ε_{ij} modeling, is computed with a transport equation for ε.

2.3. Temperature and Chemical Species Fields

The turbulent heat transfer and species transport are modeled following the Boussinesq's turbulent diffusion concept. Equation (7) and Eq.(8) represent the energy and species transport equations respectively.

$$\frac{\partial(\rho u_j h)}{\partial x_j} = \frac{\partial}{\partial x_j}\left[\left(\frac{\mu}{Pr} + \frac{\mu_t}{Pr_t}\right)\frac{\partial h}{\partial x_j}\right] + u_j\frac{\partial P}{\partial x_i}$$ (7)

$$\frac{\partial(\rho u_j m_p)}{\partial x_j} = \frac{\partial}{\partial x_j}\left[\left(\frac{\mu}{Sc} + \frac{\mu_t}{Sc_t}\right)\frac{\partial m_p}{\partial x_j}\right]$$ (8)

where h is the enthalpy and m_p is the pollutant mass fraction.

2.4. Turbulence Modeling at Walls

The turbulence treatment for the dependent variables at walls was considered by two different approaches: the logarithmic wall function, and the two-layer zonal treatment. In the first approach, logarithmic wall functions were employed for setting up the conditions for all dependent variables close to the solid boundary, following the procedure described in Launder and Spalding (1974).

In the two-layer zonal model the viscosity affected near-wall region is completely resolved all the way to the viscous sublayer. It is used to specify both the dissipation rate (ε) and the turbulent viscosity in the near-wall cells. In this approach, the whole domain is subdivided into a viscosity-affected region and a fully-turbulent region. Accordingly to (Fluent User's Guide, 2003), the demarcation of the two regions is determined by a wall-distance-based, turbulent Reynolds number, defined as

$$\text{Re}_y \equiv \frac{\rho_a y \sqrt{k}}{\mu_a}$$ (9)

where y is the normal distance from the wall at the cell centers. In the fully turbulent region $(\text{Re}_y > 200)$, the $k-\varepsilon$ or the rsm is employed. In the viscosity-affected near wall region $(\text{Re}_y < 200)$, the one-equation model of Wolfshtein (1969) is employed.

The Reynolds stresses at the wall-adjacent cells are computed from

$$\frac{\overline{u_\tau'^2}}{k} = 1.098 \ , \frac{\overline{u_\eta'^2}}{k} = 0.247 \ , \qquad \frac{\overline{u_\lambda'^2}}{k} = 0.655 \ , \qquad -\frac{\overline{u_\tau' u_\eta'}}{k} = 0.255$$ (10)

using a local coordinate system, where τ is the tangential coordinate, η is the normal coordinate, and λ is the binormal coordinate.

3. Simulation Set-up

The computational simulations intended to reproduce the conditions from a wind tunnel experiment for which the experimental data was available (Boçon and Maliska, 1998). Details of the laboratory experiments are given by Boçon, (1998); here we summarize only some important features. In those flow and pollutant dispersion laboratory experiments, axisymmetric mountain topographies were employed with the following profile:

$$z(r) = \frac{h}{1 + (r/200)^4} \tag{11}$$

where h corresponds to mountain maximum height.

Figure 1 presents the scheme employed in the simulations. There is an imposed flow at the inlet of the computational domain, and the pollutant injection is positioned $500\,mm$ upstream of the mountain top. The flow outside from the boundary layer is characterized by the velocity U_∞, ΔT represents the difference between the ground temperature (T_0) and the temperature far from the ground (T_∞).
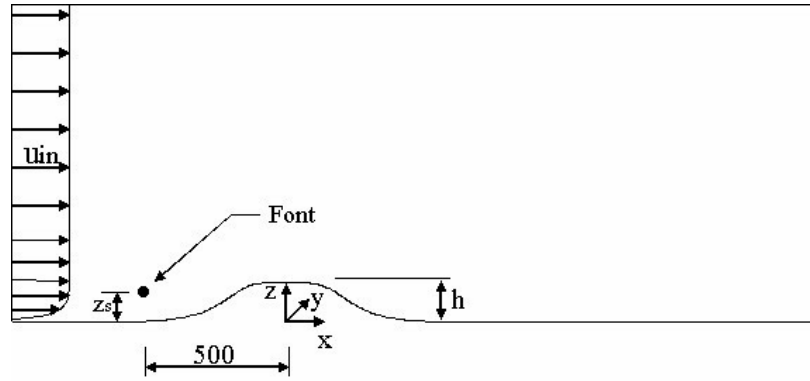
Figure 1. Simulation scheme.

Among the several cases investigated in the laboratory experiments, case E1, following the nomenclature adopted in Boçon (1998), corresponds to stable atmosphere ($\Delta T = 20^o C$, Pasquill class E) and $U_\infty = 1m/s$. In this case (E1), which was the one chosen for the present computational investigation, the source tracer gas was positioned at $(x, y, z) = (-500mm, 0, 50mm)$ for hill height $h = 100mm$.

3.1. Grid

Taking advantage of the symmetry of the problem with respect to the $y = 0$ plane, only half $(y > 0)$ of the real problem was simulated. Different computational grids were employed for the flow and concentration simulations. Both grids were developed with the software Gambit (version 2.0.4).

Figure 2 represents a $63 \times 27 \times 27$ computational grid employed in the flow solution. The computational domain for the flow solution has dimensions of $2500 \times 1000 \times 1000\,mm$ in the x, y and z directions respectively. Direction x corresponds to the main flow direction, y is transversal to the flow and z is the vertical direction. The coordinate system origin is positioned at the mountain center at ground level. For the mountain profile it was used $h = 100mm$. In the flow solution when the two-layer approach was applied, a similar grid was employed, but then the grid was even more refined close to the inferior boundary.
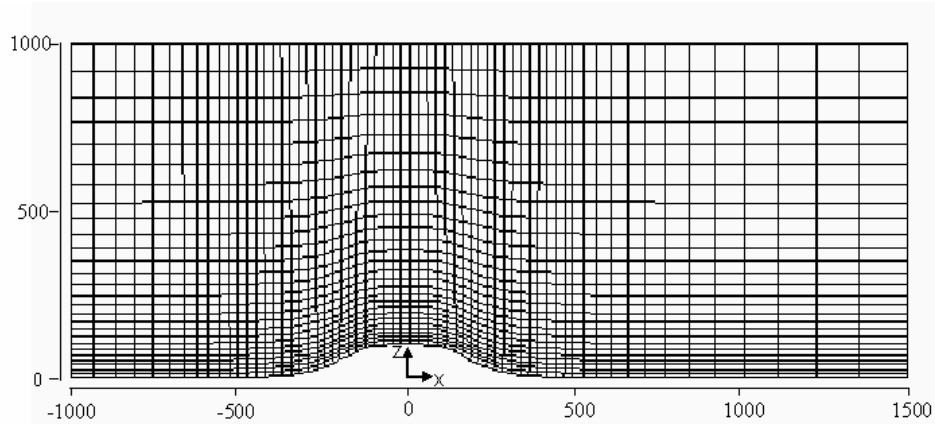
Figure 2. Flow solution grid (lateral view)

Figure 3 below represents the grid composed by $96 \times 48 \times 48$ control volumes employed on the species concentration calculations. The computational domain for the flow solution has dimensions of $2000 \times 500 \times 500\,mm$ in the x, y and z directions respectively. A rectangular section of $0.75\,mm$ in y direction and $1.5\,mm$ in z direction was defined for the pollutant injection representation. The grid is refined in the injection region and also close to the wall, where the greatest gradients are localized.
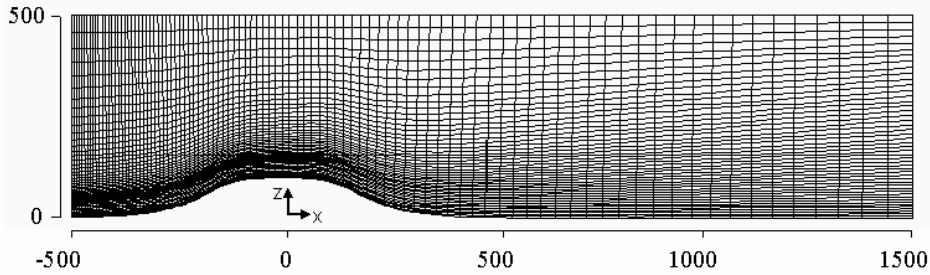
Figure 3. Concentration grid (lateral view)

3.2. Boundary Conditions

For the flow solution, inlet profiles for the velocity, temperature, turbulent kinetic energy, turbulent dissipation rate, and Reynolds stresses (when employing the *rsm*) were prescribed. The profiles for u, k e T were developed from wind tunnel measurement data, and we obtained them from (Boçon, 1998). As the dissipation rate of turbulent kinetic energy was not measured during the experiment, its inlet profile was calculated according to a prescribed turbulence length scale following the same procedure described in (Boçon, 1998). The Reynolds stresses at the inlet were obtained from the assumption of isotropy of turbulence

$$\overline{u_i'^2} = \frac{2}{3}k \tag{12}$$

$$\overline{u_i' u_j'} = 0 \tag{13}$$

where $\overline{u_i'^2}$ is the normal Reynolds stress component in each direction.

For the domain corresponding to the concentration grid, the inlet boundary condition employed was the prescription of pollutant mass fraction at the cell faces representing the font. At the other faces at the inlet boundary it was prescribed a zero pollutant mass fraction.

The lower boundary was considered as impermeable wall. The turbulence treatment for the dependent variables at the wall was considered by two different approaches: the logarithmic wall function and the two-layer zonal treatment (see section 2.4). The wall was considered non absorbing to pollutant, so the gradient concentration was considered zero at the wall.

At the lateral and upper boundaries, it was considered that the flow was not disturbed by the presence of the mountain so that the flux normal to the boundary for all scalars was set as zero. To assure the non perturbation condition, the boundaries were positioned far enough from the mountain. In the same way, the concentration flux normal to these boundaries was set as zero. Outflow conditions were those of well-developed flow; i.e. zero longitudinal gradient.

3.3. Cases for Investigation

Four different combinations of turbulence models and turbulence near-wall treatments were defined for testing and investigation:

- KE-WF is the combination that includes the $k - \varepsilon$ model for turbulence and the wall logarithmic function for the turbulence treatment at walls.
- RSM-WF is the combination that includes the Reynolds stress model for turbulence and the wall logarithmic function for the turbulence treatment at walls.
- KE-2L is the combination that includes the $k - \varepsilon$ model for turbulence and the two-layer zonal model for the turbulence treatment at walls.
- RSM-2L is the combination that includes the Reynolds stress model for turbulence and the two-layer zonal model for the turbulence treatment at walls.

The different combinations above were employed in the simulation of the flow and the results were plotted for comparison purpose.

For the concentration field calculation, the flow solution was interpolated to adapt it to the concentration grid. In this domain, only the species transport equation (Eq.8) was solved. Therefore, the KE-WF*, RSM-WF*, KE-2L* and RSM-2L* nomenclature here defines the original flow field employed in the concentration calculation.

For the comparison with the experimental data, the calculated concentration C (kg / m^3) was transformed into

$$C^* = \frac{U_\infty C}{Q} \qquad (m^{-2}) \tag{14}$$

where Q is the font intensity (kg / s).

4. Results:

4.1. Flow Results

Figure 4 represents horizontal velocity (u) profiles in several x positions along the symmetry plane $(y = 0)$ corresponding to case E1 (defined in section 3). In general, it can be observed that the numerical results agree reasonably well with the experimental data. In positions $x = -200mm$ and $x = 0$, the numerical results are very similar, but in positions $x = 250mm$ and $x = 500mm$ they present significant differences.

At position $x = 250mm$ it can be noted that the combinations of turbulence model and near-wall treatment, as defined in the previous section, including two-layer zonal treatment presented better results than those including the wall function when compared to the experimental data. The first combinations were able to predict the recirculation of the flow (negative velocities) that occurs at the lee-side of the mountain, as appointed by the experimental results. Among the combinations including the two-layer zonal treatment, the results from the RSM-2L velocity prediction were closer to the experimental data than the ones from the KE-2L prediction.

The better performance of the RSM-2L combination can be again verified in the figure corresponding to the position $x = 500mm$. In this figure the results from RSM-2L are closer to the experimental results than those obtained by the other combinations in the near-wall region.

Figure 5 presents the turbulent kinetic energy (k) profiles in several x positions along the symmetry plane $(y = 0)$ referent to case E1. In the plots corresponding to the positions $x = -200mm$ and $x = 0$, it can be noted that, except by the near-wall region, the numerical results agree satisfactorily with the experimental data. It is also in the near wall region that divergences in the numerical results from the different combinations are more evident.

At positions $x = 250mm$ and $x = 500mm$, which are located downstream of the mountain, the comparison between the numerical and experimental results shows that the RSM-2L and KE-2L combinations could predict the increase of the turbulent kinetic energy (k) close to the wall, but the other combinations could not. In position $x = 500mm$ it can be verified that the combination RSM-2L is the one that better predicts the trend on the increase of the turbulent kinetic energy

(k) close to the wall. In general, it could be observed that the combinations employing the two-layer zonal treatment presented better performance than those which applied the wall functions.

It is well established that the eddy viscosity models do not correctly mimic the sensitivity of the turbulent stresses with respect to streamline curvature and body forces (Launder, 1989). From the calculation of the transport equations for $\overline{u_i u_j}$, second–moment closure offers a more reliable approach for predicting complex flows than eddy-viscosity-based model. The complex flow investigated in the present work presents streamline curvature and a separation zone. Also, the Reynolds stress model capability in reproducing anisotropic turbulent diffusion explains the superior results obtained here by the employment of such modeling approach. In stably stratified flows, the turbulent vertical fluctuations are inhibited. These anisotropic effects, produced by significant temperature gradient, cannot be adequately represented by isotropic models like the standard $k - \varepsilon$.

When employing the two-layer zonal treatment, the viscosity-affected near-wall region is completely resolved all the way to the viscous sublayer. It is expected that this treatment makes it possible to predict, with more accuracy, the flow characteristics in the near-wall region. The superior performance presented by the RSM-2L combination could be justified by these special features of the Reynolds stress model and the two-layer zonal treatment.
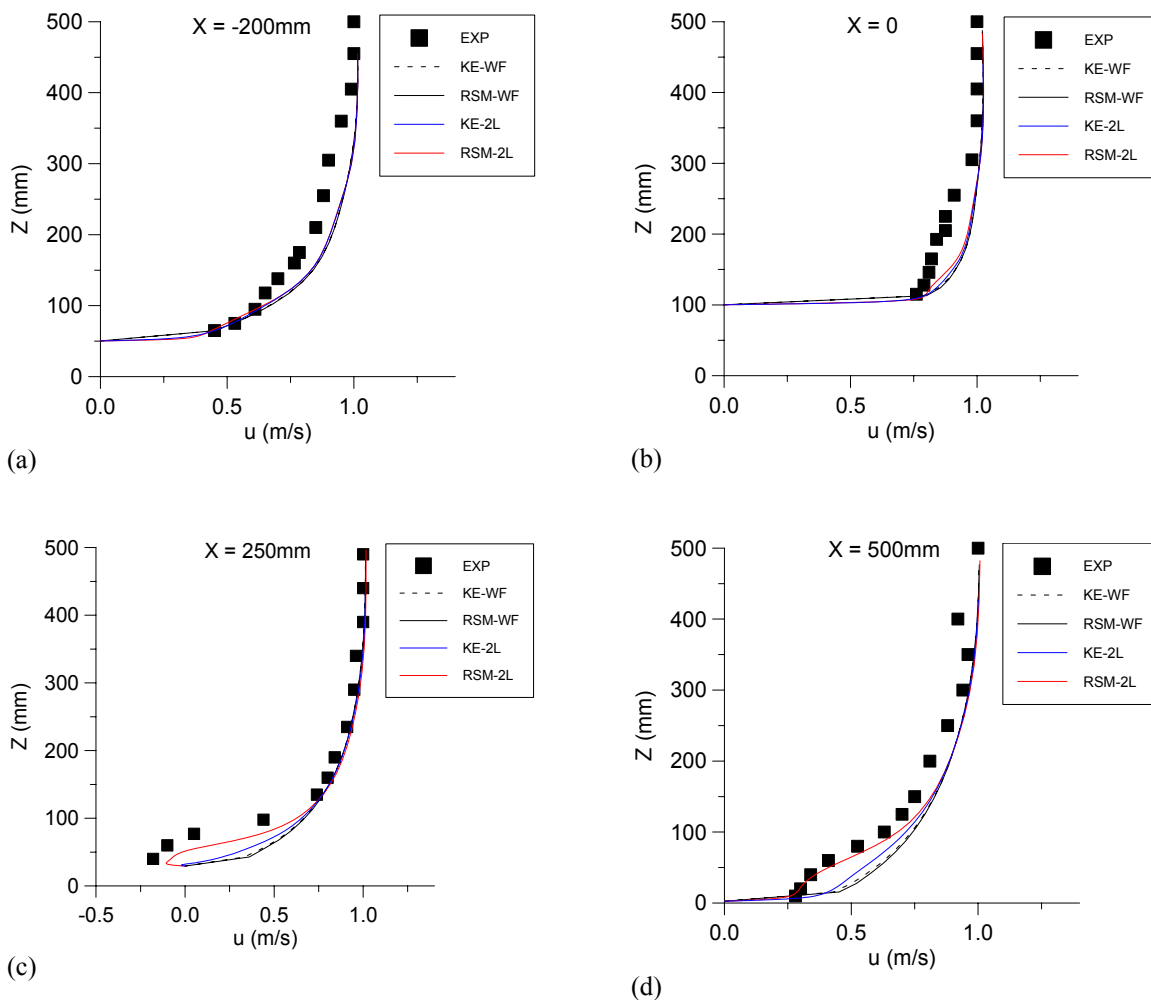
Figure 4. Vertical profiles of (u) velocity component at the symmetry plane $(y = 0)$ for different x positions: (a) $x = -200mm$, (b) $x = 0$, (c) $x = 250mm$ and (d) $x = 500mm$.
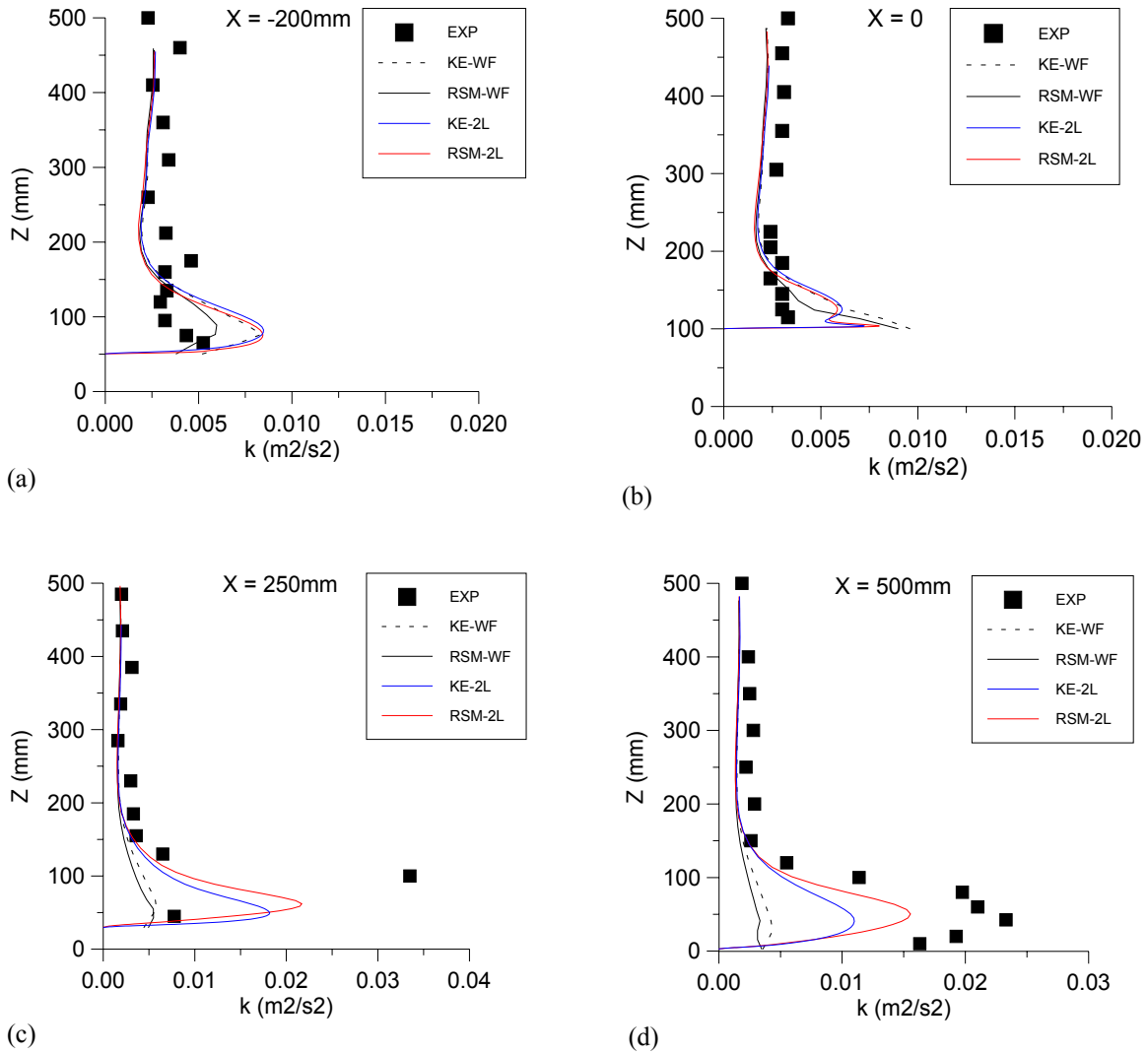
Figure 5. Vertical profiles of turbulent kinetic energy (k) at the symmetry plane $(y = 0)$ for different x positions: (a) $x = -200mm$, (b) $x = 0$, (c) $x = 250mm$ and (d) $x = 500mm$.

4.2. Concentration Results

Figure 6 presents comparisons between the calculated concentration profiles and the experimental data for the E1 case. At positions $x = -200mm$ and $x = 0$, it can be noted that the results referent to the numerical curves corresponding to the combinations KE-2L* and RSM-2L* are practically the same. The numerical models investigated couldn't predict adequately the concentration reduction that occurs close to the wall for the positions $x = -200mm$ and $x = 0$. At the ground level, the numerical curves present concentration levels higher than those obtained experimentally.

At positions $x = 200mm$ and $x = 500mm$, the numerical curves show the models difficulty in calculating the concentrations close to the wall. However, it can be observed that the concentration fields, obtained from the flow solutions in which the two-layer zonal treatment was applied, were more realistic than the others. The RSM-2L* and KE-2L* numerical results approximate to the experimental data with the downwind distance growth.

Although the Reynolds stress model performance was superior in predicting the flow solution, the predictions for the concentrations calculated from the flow field solutions, obtained by employing the *rsm* and the $k - \varepsilon$ model, was practically the same. This could be verified by the comparison between the KE-

2L* and RSM-2L* results, and between the KE-WF* and RSM-WF* results. The more reliable description of the velocity and turbulent kinetic energy fields obtained by the *rsm*, presented in Figs. (4) and (5), did not reflect in more accurate concentration calculations. The concentration results show that the isotropic eddy-viscosity approach, applied in the present work for the concentration transport calculations, cannot adequately predict absolute values of ground-level concentration from the plume submerged within the complex flow investigated. The use of the same diffusivity in the vertical and lateral directions does not provide a representative description for the corresponding real turbulent diffusion. Therefore, a better description of the anisotropy in turbulent exchanges is necessary for the concentration calculations.

(a)

(b)

(c)

(d)
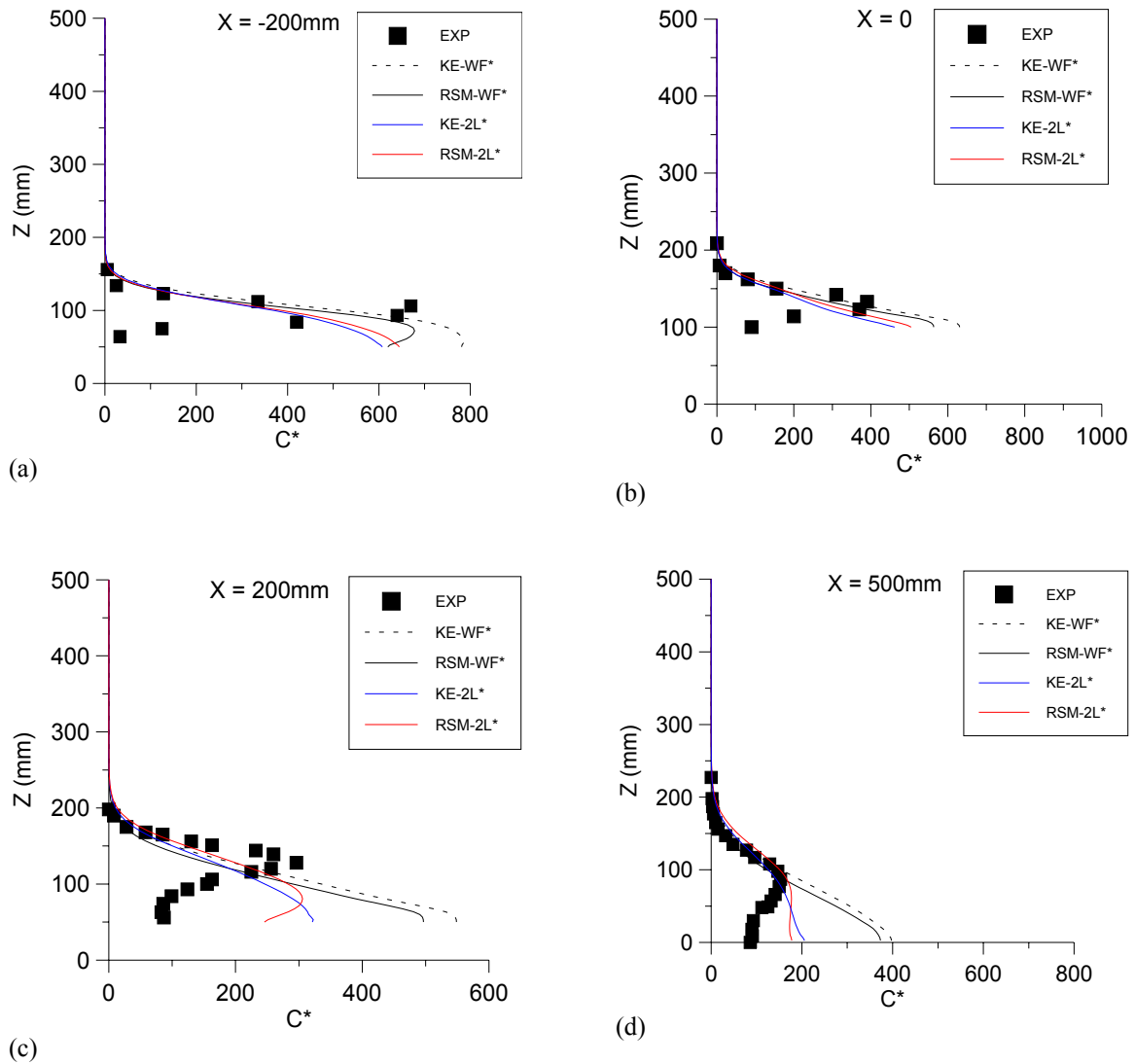
Figure 6. Vertical profiles of concentration C^* at the symmetry plane $(y = 0)$ for different x positions: (a) $x = -200mm$, (b) $x = 0$, (c) $x = 200mm$ and (d) $x = 500mm$. The KE-WF*, RSM-WF*, KE-2L* and RSM-2L* nomenclature here defines the original flow field employed in the concentration calculation.

However, the superior performance in predicting the flow solution, obtained by employing the two-layer zonal treatment, was also responsible for a better prediction of the concentrations, in comparison with the flow solutions obtained by employing the wall functions. In fact, the choice for the treatment of the near wall turbulence (wall function or two-layer treatment) in the flow calculations produced more significant

effects on the concentrations results than the turbulence model (rsm or $k-\varepsilon$). Observing Figs. (5c) and (5d) again, it can be noted that the divergences between the numerical curves for k were more sensitive to the choice of the near wall turbulence treatment than to the turbulence model choice. This explains why the concentration calculations were more influenced by the near-wall turbulence treatment in the flow solution than by the choice between the rsm and the $k-\varepsilon$ models.

5. Conclusion

The Reynolds stress model was applied to simulate stratified atmospheric flows over an idealized three dimensional topography and results were compared to experimental data and to the numerical results obtained by the $k-\varepsilon$ model. Also, a two-layer zonal model was implemented for the near-wall treatment and the results were compared to the ones obtained with the logarithmic wall function. The pollutant dispersion was simulated by assuming an isotropic eddy-viscosity approach.

The flow solution was better predicted by the employment of the Reynolds stress model and the two-layer treatment, which resulted in a more realistic representation of the recirculation zone which is present in the lee side of the hill. Although the Reynolds stress model performance was superior in predicting the flow solution, this superiority did not result in more accurate concentration calculations. The predictions for the concentrations calculated from the flow field solutions obtained by the employment of the rsm and the $k-\varepsilon$ model were practically the same. The isotropic eddy-viscosity approach applied in the concentration calculations cannot adequately predict values for ground-level concentration. However, when it was employed the two-layer zonal treatment in the flow solution, the concentration results were closer to the experimental data than those where it was employed the logarithmic wall law. This occurred mainly in the region downstream to the mountain.

6. Acknowledgement

7. References

Apsley, D.D. and Castro, P.I., 1997, "Numerical Modeling of Flow and Dispersion around Cinder Cone Butte", Atmospheric Environment, vol.31, no 7, pp. 1059-1071.

Boçon, F.T. and Maliska, C.R., 1998, "Application of a Non Isotropic Model to Stable Atmospheric Flows Over 3D Topography", Proceedings of the 7th Brazilian Congress of Engineering and Thermal Sciences, Rio de Janeiro, Brazil, vol. 2, pp. 1334-1339.

Boçon, F.T., 1998, "Modelagem Matemática do Escoamento e da Dispersão de Poluentes na Microescala Atmosférica", Tese de Doutorado, Universidade Federal de Santa Catarina, Florianópolis, Brazil.

Boçon, F.T. and Maliska, C.R., 1999, "Numerical Study of 3D Atmospheric Pollutant Dispersion Over Real Terrain", Proceedings of the 15th Brazilian Congress of Mechanical Engineering, Águas de Lindóia, Brazil, published in CD-ROM.

Castro, P.I. and Apsley, D.D., 1997, "Flow and Dispersion Over Topography: A Comparison Between Numerical and Laboratory Data for Two-Dimensional Flows", Atmospheric Environment, vol. 31, no 6, pp. 839-850.

Fluent User's Guide, v. 6.0.12, 2003, Fluent Inc., New Hampshire.

Isnard, A.A. and Gomes, M.S.P., 2002, "CFD Investigation on Pollutants Dispersion at the Atmospheric Microscale", Proceedings of the 9th Brazilian Congress of Engineering and Thermal Sciences, Caxambu, Brazil, published in CD-ROM.

Launder, B.E. and Spalding, D.B., 1974, "The Numerical Computation of Turbulent Flows", Computer Methods in Applied Mechanics and Engineering, 3, p.269-289.

Launder, B.E., 1989, "Second-Moment Closure and Its Use in Modeling Turbulent Industrial Flows", International Journal for Numerical Methods in Fluids, 9:963-985.

Wolfshtein, M., 1969, "The Velocity and Temperature Distribution in One-Dimensional Flow with Turbulence Augmentation and Pressure Gradient", International Journal of Heat and Mass Transfer, vol. 12, pp. 301-318.